Chronic lung inflammation and pulmonary fibrosis after multiple intranasal instillation of PM2.5 in mice

Mengmeng Xu
First Affiliated Hospital of Anhui Medical University
Hai Zhang
Shanghai Jiao Tong University Affiliated Chest Hospital
Lu Xu
First Affiliated Hospital of Anhui Medical University
Xiaohui Wang
Shanghai Jiao Tong University Affiliated Chest Hospital
Chenfei Li
Shanghai Jiao Tong University Affiliated Chest Hospital
Yuqing Chen
Shanghai Jiao Tong University Affiliated Chest Hospital
Kian Fan Chung
Imperial College London
Ian M Adcock
Imperial College London
Li Feng (lifeng741@aliyun.com)
Shanghai Jiao Tong University Affiliated Chest Hospital

Research

Keywords: Pulmonary Fibrosis, PM2.5, TGFβ1, Epithelial-mesenchymal transition, Mitochondrial damage, Mitophagy

Posted Date: February 12th, 2020

DOI: https://doi.org/10.21203/rs.2.23313/v1

Abstract

Background: Fine particulate matter (PM 2.5) is an important component of air pollution and can induce lung inflammation and oxidative stress. We hypothesised that PM 2.5 could play a role in the induction of pulmonary fibrosis. We examined whether multiple intranasal instillation of PM 2.5 can induce pulmonary fibrosis in the mouse, and also investigated the underlying pro-fibrotic signaling pathways.

Methods: C57/BL6 mice were intranasally instilled with 50 μl of PM 2.5 suspension (7.8 μg/g body weight) or PBS three times a week over 3 weeks, 6 weeks or 9 weeks. To observe the recovery of pulmonary fibrosis after the termination of PM 2.5 exposure, 9 week-PM 2.5 instilled mice were also studied at 3 weeks after termination of instillation.

Results: There were significant decreases in total lung capacity (TLC) and compliance (Cchord) in the 9-week PM 2.5 -instilled mice, while there was an increase in total cell counts in bronchoalveolar fluid and lung section in 3-week, 6-week and 9-week PM 2.5 -instilled mice and 9 week-PM 2.5 instilled-3 week-air exposed mice. There were increased histological fibrosis scores with enhanced type I collagen and hydroxyproline deposition in lung tissue in 6-week and 9-week PM 2.5 -instilled mice and 9-week-PM 2.5 instilled-3-week-air-exposed mice. Multiple PM 2.5 instillation resulted in increased expression of TGFβ1, increases of N-Cadherin and Vimentin and decrease of E-Cadherin. It also led to decreases in OPA1 and MFN2, and increases in Parkin, SQSTM1/p62, the ratio of light china (LC) 3B II to LC3B I, PI3k/Akt phosphorylation, NOX4 and NLRP3 expression.

Conclusions: The intranasal instillation of PM 2.5 for 9 weeks induced lung inflammation and pulmonary fibrosis, which was linked with aberrant epithelial-mesenchymal transition, mitochondrial damage and mitophagy, as well as activation of TGFβ1-PI3K/Akt and TGFβ1-NOX4 -NLRP3 pathways.

Background

Idiopathic pulmonary fibrosis (IPF) is a chronic, progressive and fibrotic interstitial pneumonia of unknown cause [1]. It is a rare and poor-prognosis disease, with global incidence of 3–9 cases per 100 000 person-year [2], and median survival time of 2–4 years after diagnosis [3]. Clinically, it is characterized by worsening symptoms including dyspnoea, cough and progressive loss of lung function. Pathologically, it is characterized by patchy dense fibrosis that causes remodeling of lung architecture and honeycomb change [1]. The aetiology of IPF is complex and may include male, old age, cigarette smoke, gastroesophageal reflux, chronic viral infections and genetic factors [1]. Air pollution, an increasing problem worldwide with serious health implications, has been recognized to be an important risk for the development and acute exacerbation of IPF [4, 5].

Although the pathogenesis of IPF is not completely clear, repetitive micro-injuries to alveolar epithelium play a central role in the formation of pulmonary fibrosis. The injured alveolar epithelial cells can secrete chemokines to recruit inflammatory cells such as monocytes/macrophages and neutrophils to the site of injury, and then these cells produce reactive oxygen species (ROS), pro-fibrotic cytokines and mediators

[6]. Simultaneously, damaged alveolar epithelial cells, especially type 2 alveolar epithelial cells, can induce the differentiation of fibroblasts into myofibroblasts and initiate the fibrotic process through a process of epithelial–mesenchymal transition (EMT) [7]. The myofibroblasts deposit increases and alters extracellular matrix (ECM), with altered biomechanical stiffness, which further contributes to myofibroblast activation.

Transforming growth factorβ (TGFβ) superfamily, in which TGFβ1 is the most notable and extensively studied isoform, is a pivotal pro-fibrogenic factor that can accelerate EMT, promote fibroblast proliferation, increase ECM deposition, induce lung structural remodeling[8], and activate pro-fibrotic pathways, such as TGFβ1-PI3K/Akt [9], TGFβ1- NADPH oxidase(NOX)4 [10] and TGFβ1-NLRP3 [11] pathways.

IPF is an aging-related disease, and aging particularly affects mitochondria [12]. As one of most important organelles in the cell, mitochondria are involved in energy production by oxidative phosphorylation and other metabolic processes in order to maintain intracellular homeostasis, in which mitochondrial dynamics (fusion/fission) and mitochondria-specific autophagy known as mitophagy are two main machineries [13]. The imbalance of mitochondrial dynamics will cause over-production of mitochondrial ROS (mtROS) and aberrant mitophagy, and further induce pro-fibrotic responses [14]. Similarly, impairment of mitophagy is associated with increased ROS production, ECM deposition and TGFβ1 expression, which all enhance myofibroblast transformation [12].

Fine particulate matter (with an aerodynamic diameter < 2.5 μm, $PM_{2.5}$) is a major air pollutant. $PM_{2.5}$ can be inhaled into lung, deposit in distal small airways and alveoli, accumulate in lung parenchyma, and result in pulmonary inflammation and oxidative stress as it induces the release of ROS and fibrogenic factors such as TGFβ1 from lung epithelial cells [15]. We have demonstrated that acute exposure of $PM_{2.5}$ induces the activation of the NLRP3/caspase-1 pathways as well as dysregulation in mitochondrial fusion/fission proteins in vivo and in vitro [16]. Recent studies showed that exposure to $PM_{2.5}$ in mice increased the expression of α-smooth muscle actin (α-SMA) and TGFβ1 and promoted pulmonary fibrosis [17, 18].

We hypothesised that long-term exposure to $PM_{2.5}$ could lead to pulmonary fibrosis. We therefore examined whether multiple intranasal instillation of $PM_{2.5}$ induces pulmonary fibrosis in mice, and if so, we further analysed the potential pro-fibrotic signaling pathways induced by $PM_{2.5}$.

Materials And Methods

$PM_{2.5}$ Sampling, extraction and analysis

$PM_{2.5}$ samples were collected on the top of an office building in Xuhui, Shanghai, China, using High Flow $PM_{2.5}$ Sampler (Ecotech, Australia) at a flow rate of 1.13 m^3/min between August 2017 and June 2018. The sampling, extraction and analysis were performed according to our previous study [16]. In brief,

$PM_{2.5}$ fiber filters were sheared into small fragments, immersed into ultrapure water which was eluted with an ultrasonic cleaner, followed by filtrating, freezing and vacuum drying. Finally, $PM_{2.5}$ solid particulates were collected and conserved at -20°C. $PM_{2.5}$ solid particulates were evenly suspended in phosphate buffer saline (PBS) by vortex concussion and stored at 4°C before the intranasal instillation.

The metal contents were determined by inductively coupled plasma optical emission spectrometer (ICP-OES) analysis with an Agilent ICP-OES 5110 instrument. The inorganic anions (e.g., F^-, $NO3^-$, Cl^- and $SO4^{2-}$) and cations (e.g., Na^+, $NH4^+$, K^+, Ca^{2+}, and Mg^{2+}) of the solid particulates were analyzed using an Ion Chromatography system (Dionex ICS-5000+/900, Thermo Fisher, Darmstadt, Germany). TOC was measured using a total organic carbon (TOC) analyzer (Vario EL Cube, Elementar, Germany). For the analysis of Poly aromatic hydrocarbons (PAHs) in $PM_{2.5}$, the particulates were sonicated in 5 mL dichloromethane (DCM)/methanol (2:1, v/v) mixture 30 min three times, then the total extractive liquid was concentrated to approximately 1 mL by rotary evaporator and then blown to 200 μL under a gentle stream of nitrogen. Finally, the methylated particles were analyzed with a gas chromatography-mass spectrometer (GCMS-QP2020, Shimadzu Corporation, Otsushi Shiga, Japan).

Mice and treatments

All experimental studies involved mice were approved by the laboratory animal ethics committee of the Shanghai Chest Hospital, Shanghai, China (Approval number: SYXK 2018-0016). Fifty-six 8-week-old male C57/BL6 mice, weight 22-25 g, were provided by Shanghai Super–B&K Laboratory Animal (Shanghai, China). Mice were fed in specific pathogen-free house where the circulating temperature is at 22°C with 50-60% humidity, equally light-dark cycle and standard diet.

After inhalation of isoflurane as anesthetic, mice were intranasally instilled with $PM_{2.5}$ particulates (7.8 μg/g) suspended in 50 μL of PBS or vehicle (PBS), three times a week, over 3 weeks, 6 weeks and 9 weeks. Mice were studied 24 h after the last instillation to $PM_{2.5}$. To observe the recovery of pulmonary fibrosis after the termination of $PM_{2.5}$ exposure, another group of 9-week $PM_{2.5}$ instilled mice were studied after 3-week of the last instillation.

Lung function detection

After anesthesia with an intraperitoneal injection of 0.2 ml 1% pentobarbital, mice were tracheostomized and placed in a whole-body plethysmograph (EMMS, Hants, UK). Inspiratory capacity (IC), total lung capacity (TLC), and forced vital capacity (FVC) were recorded during fast flow volume maneuver from quasi-static pressure-volume loops. The chord compliance (Cchord) was determined from the quasi-static pressure-volume maneuver. Three acceptable maneuvers were conducted for each test in every mouse.

Collection and measurement of bronchoalveolar lavage (BAL) fluid and serum

Following terminal anaesthesia with 0.4 ml pentobarbitone, mouse bronchoalveolar lavage (BAL) fluid and blood were collected. Total and differential cell counts in BAL fluid were measured by two blinded

and independent observers. At least 500 cells were counted and identified as macrophages, eosinophils, lymphocytes or neutrophils according to standard morphology.

TGFβ1 in serum was assayed using mouse TGFβ1 ELISA kit (Mutisciences, Hangzhou, China) following the instructions from the manufacturer.

Histological Analysis

The left lung was inflated with 4% paraformaldehyde under 25 cm of water pressure and then embedded in paraffin. Paraffin blocks were sectioned to expose the maximum surface area of lung tissue in the plane of the bronchial tree. Four μm sections were cut and stained respectively with haematoxylin and eosin (H&E), Masson trichrome stain and Sirius red stain.

The mean linear intercept (Lm), a measure of interalveolar septal wall distance, and the extent of lung inflammation score were determined respectively in H&E-stained lung sections the as described previously [19].

The extent of lung inflammation was scored in the H&E-stained lung sections according to the method described by Szapiel SV [20].

The severity of pulmonary fibrosis was assessed in the Masson trichrome-stained sections, and Ashcroft scoring was measured as described before [21].

Airway subepithelial collagen deposition was estimated in Masson trichrome stained sections, and the thickness of collagen deposition was calculated by dividing the area of airway subepithelial collagen deposition by the perimeter of airway basement membrane. Type I and type III collagen in mouse lung tissues were determined by using the Sirius red stain [22]. Under polarized light microscopy, the type I collagen in sections is shown as yellow-orange, while the type III collagen is shown as green. Quantification of type I collagen was performed by calculating the overall area of both occupied area and color depth in the lung sections using an image J analysis system. The results are reported as mean %area of yellow-orange in Sirius-red stained sections.

Hydroxyproline assay

The hydroxyproline content in lung tissues were measured by the alkaline hydrolysis using a hydroxyproline kit (Nanjing Jiancheng Institute, China). According to the instructions, fresh lung tissues were weighed and alkaline hydrolyzed for 20 min at 100℃, adjusting pH of hydrolysates to 6.0-6.8, then adding active carbon and centrifuging the suspension. After a series of chemical reactions, the supernatants were obtained to detect OD value at 550 nm, and the results were expressed as micrograms of hydroxyproline per gram of wet lung weight (μg/g) by comparing with HYP standards.

Immunohistochemistry

The localization and expression of TGFβ1 in lung tissues were examined by immunohistochemical staining. Lung sections were incubated with anti-TGFβ1 primary antibody (1:500 in PBS, Abcam Cambridge, MA, USA), polyclonal goat anti-rabbit horseradish peroxidase-conjugated secondary antibody followed by visualized with diaminobenzidine (DAB) liquid and counter-stained with hematoxylin. The brown staining intensity for TGFβ1 in lung tissues was scored on 0-3 scale [16].

MtROS assay

The mitochondria of fresh lung tissues were extracted with Tissue Mitochondria Isolation Kit (Beyotime technology, Haimen, Jiangsu, China), and then re-suspended with mitochondrial stock solutions. Immediately, mitochondrial suspension was quantified and then incubated with 5 μM MitoSOX working solution (Invitrogen, USA) for 10 min at 37°C, protected from light. MitoSOX fluorescence was measured by Varioskan Flash (Thermo Sciectific, USA) at wavelengths of 510 nm for excitation and 580 nm for emission.

Western blot analysis

Total proteins were extracted from mouse lung tissues with RIPA lysis buffer (Beyotime technology, China), and protein concentrations were quantified by Pierce BCA assay kit (Thermo Fisher Scientific, Waltham, MS, USA). Equal amounts of lung homogenate or mitochondrial extract were separated through 10-15% denaturing polyacrylamide gels (Beyotime technology) and transferred to PVDF membranes. The membranes were blocked with 5% nonfat dry milk and incubated overnight at 4°C with the following primary antibodies: N-Cadherin, Vimentin, E-Cadherin, dynamin-related protein 1(DRP1), mitochondrial fission factor (MFF), mitofusin2 (MFN2) and optic atrophy 1 (OPA1), phospho-PI3K, total PI3K, phosphor-Akt, total Akt, NLRP3, GAPDH (all from Cell signaling technology, Danvers, MA, USA), TGFβ1, PINK1, Parkin, LC3B and SQSTM1/p62 (all from Abcam), NOX4 (Novus, Littleton, Colorado, USA). Then membranes were incubated with an HRP-conjugated anti-rabbit secondary antibody (Cell Signaling Technology), and then visualized by chemiluminescent detection.

Statistical analysis

Data are presented as mean ± SEM. Multiple-group comparisons were analyzed using one-way ANOVA by Bonferroni's post hoc test (for equal variance) or Dunnett's T3 post hoc test (for unequal variance). $P < 0.05$ was considered statistically significant.

Results

Biochemical analyses of $PM_{2.5}$

The analyzed results showed there were numerous metal elements, metal ions, oxidizing ions, toxic PAHs in $PM_{2.5}$ samples (Table 1).

Biochemical analyses of PM2.5.

Chemical element (mg/g)		PAH (ug/g)		Anions (mg/g)	
Fe	10.745	Naphthalene	0.537	F^-	0.504
Zn	1.591	1-Methyl naphthalene	0.371	Cl^-	10.940
Cr	0.164	2-Methyl naphthalene	0.163	Br^-	0.042
Pb	0.682	Acenaphthylene	0.231	NO_3^-	65.271
Ce	0.9	Acenaphthene	0.050	SO_4^{2-}	48.108
As	0.036	Fluorene	0.114	PO_4^{3-}	0.111
Cu	0.373	Phenathrene	0.046	TOC (%)	
Mn	0.518	Anthracene	1.242	TOC	17.01
Ti	0.145	Fluoranthene	2.691		
Ba	0.245	Pyrene	1.481		
Mg	1.636	Benzo[a]anthracene	0.528		
Cations (mg/g)		Chrysene	4.005		
Ca^{2+}	8.615	Benzo[a]pyrene	81.404		
Na^+	6.873	Dibenzo[a,h]anthracene	84.989		
K^+	3.687	Benzo[b]fluorathene	64.797		
NH_4^+	23.353				

Table 1: Total organic carbon (TOC) (%) represents the proportion of TOC in the qualitative $PM_{2.5}$ samples. PAHs: Polycyclic aromatic hydrocarbons.

Lung function measurements

Compared to control mice, there were decreases in TLC and Cchord in 9-week $PM_{2.5}$-instilled mice, and there was a decrease in IC in 6-week and 9-week $PM_{2.5}$-instilled mice, with no change in FVC. Furthermore, TLC remained reduced in 9-week $PM_{2.5}$-instilled 3-week air-exposed mice (Fig. 1A-D).

BAL fluid cells and lung inflammation scores

$PM_{2.5}$-instilled mice demonstrated significant increases in total cells, including macrophages, neutrophils, lymphocytes, and eosinophils in BAL fluid after 3-week, 6-week and 9-week of $PM_{2.5}$ instillation compared

with control mice (Fig. 2A-E). The number of total cells and macrophages remained increased in BAL fluid in 9-week $PM_{2.5}$-instilled 3-week air-exposed mice (Fig. 2A-E). There were significant increases in lung inflammation scores in 3-week, 6-week and 9-week of $PM_{2.5}$-instilled mice (Fig. 2F).

Lung histopathological analysis and hydroxyproline contents

Representative examples of lung tissue with interalveolar septal wall distance (Lm), and lung tissue with collagen deposited along the bronchus, alveolar walls and vessels (Fig. 3A-C). There was no change in Lm between all $PM_{2.5}$-instlled mice and control mice (Fig. 3D).

There were increases in fibrosis scores and collagen deposition in 6-week and 9-week $PM_{2.5}$-instlled mice and 9-week $PM_{2.5}$-instilled 3-week air-exposed mice compared with control mice (Fig. 3E and 3F). Similarly, increased type I collagen deposition percentage was observed in 6-week and 9-week $PM_{2.5}$-instlled mice and 9-week $PM_{2.5}$-instilled 3-week air-exposed mice (Fig. 3G).

To further evaluate collagen contents, hydroxyproline contents of mouse lung tissues were measured by the alkaline hydrolysis assay. Compared with control mice, the hydroxyproline contents were increased in 6-week and 9-week $PM_{2.5}$-instlled mice and 9-week $PM_{2.5}$-instilled 3-week air-exposed mice (Fig. 3H).

Oxidative stress

There was an increase in mtROS levels in 3-week, 6-week and 9-week $PM_{2.5}$-instilled mice compared with control mice (Fig. 4A). The elevated levels of NOX4 in lung tissue were found in 3-wee, 6-week and 9-week $PM_{2.5}$-instilled mice and 9-week $PM_{2.5}$-instilled 3-week air-exposed mice (Fig. 4B).

TGFβ1 expression

The expression of TGFβ1 was significantly increased after 3-week, 6-week and 9-week of $PM_{2.5}$ instillation and after 3-week of cessation, as indicated by enhanced TGFβ1 staining scores by immunohistochemistry and enhanced TGFβ1 expression by western blot in lung tissues (Fig. 5A-C). The serum TGFβ1 levels showed a trend of increasing in $PM_{2.5}$-instilled mice, and statistical significance was achieved in 9-week $PM_{2.5}$-instilled mice compared to control mice (Fig. 5D).

Biomarkers of EMT

There were significant increases in the expression of N-Cadherin and Vimentin, and a decrease in the expression of E-Cadherin and in 6-week and 9-week $PM_{2.5}$-instilled, and 9-week $PM_{2.5}$-instilled 3-week air-exposed mice compared to control mice (Fig. 6A-C).

Mitochondrial fission/fusion and mitophagy

$PM_{2.5}$ instillation led to aberrant mitochondrial fission/fusion, shown by significant increases in DRP1 and MFF expression in 3-week $PM_{2.5}$-instilled mice, and decreases in OPA1 and MFN2 expression in 9-

week $PM_{2.5}$-instilled and 9-week-3-week-air-exposed mice (Fig. 7A, 7B, and 7E-H). Moreover, 9-week $PM_{2.5}$-instilled mice demonstrated an increased expression of Parkin protein, but not PINK1, compared to control mice (Fig. 7C, 7I and 7J). There were also up-regulation in the levels of autophagy, as indicated by increased expression of SQSTM1/p62 and elevated ratio of LC3B II to LC3B I in 9-week $PM_{2.5}$-instilled, and 9-week $PM_{2.5}$-instilled 3-week air-exposed mice compared to control mice (Fig. 7D, 7K and 7L).

PI3K/Akt phosphorylation and NLRP3 expression

There were increases in the phosphorylation of PI3K and Akt after 3-week, 6-week and 9-week of $PM_{2.5}$ instillation, and after 3-week of cessation compared to control mice (Fig. 8A and 8B). Similarly, $PM_{2.5}$ instillation also promoted the expression of NLRP3 protein after 3-week, 6-week and 9-week of $PM_{2.5}$ instillation, and after 3-week of cessation compared to control mice (Fig. 8C).

Discussion

In the present study, we confirmed that intranasal instillation of $PM_{2.5}$ (7.8 μg/g), three times per week over a 9-week period induced pulmonary fibrosis in mice as measured by reduced lung function, increased collagen deposition in the lung and histological evidence of fibrosis. From 3 weeks of $PM_{2.5}$ instillation, pro-fibrotic processes were evident with non-significant increases in collagen deposition, TGFβ1 expression and EMT. However, by 9 weeks of $PM_{2.5}$ instillation, pulmonary fibrosis was observed pathologically and was accompanied by increases in EMT, mitochondrial damage and autophagy, as well as the activation of TGFβ1-PI3K/Akt, TGFβ1-NOX4-NLRP3 pathways. Thus, it takes 9 weeks of instillation to induce pulmonary fibrosis. Compared to 4-week $PM_{2.5}$-instilled mice model by Xu Z et al [18], our multi-stage $PM_{2.5}$ instillation model systematically demonstrates the development process of pulmonary fibrosis, and dynamic change in pro-fibrotic protein expression levels, as well as irreversibility of pulmonary fibrosis by $PM_{2.5}$.

The intratracheal instillation of bleomycin (BLM)-induced model represents the most common preclinical IPF model [23, 24]. The BLM-induced model has particular limitations in that it does not entirely mimic the characteristics of human IPF. For instance, the fibrosis usually develops at 21 days after BLM stimulation and spontaneously resolves at 4 weeks. However, the fibrotic change in our model was much slower, achieving a maximum effect by 9 weeks of exposure, and there was no significant recovery after 3 weeks of cessation. These indicate that $PM_{2.5}$-induced model may be more reminiscent of the clinical features of IPF than that of BLM. Moreover, intratracheal administration of BLM has considerable accumulative mortality due to the surgical operation for instillation and the high toxicity by BLM itself. The use of intranasal instillation of $PM_{2.5}$ in our study showed no mortality in the animal due to the non-invasive operation and relatively low toxicity by $PM_{2.5}$.

In the present experiment, intranasal instillation of $PM_{2.5}$ induced lung inflammation, as shown by increased macrophages, neutrophils, eosinophils and lymphocytes in BALF, and inflammatory infiltration

in peri-bronchus and peri-vascular lung tissues. The persistent inflammatory responses may contribute to the increased expression of pro-fibrotic factors and drive pulmonary fibrosis progression. In this regard, the increased recruitment of macrophages observed in the lung tissues is of interest. In particular, M1 macrophages are pro-inflammatory during the onset of injury, and M2 macrophages are pro-fibrotic and pro-healing during the chronic phase of inflammation [25]. M2 macrophages drive type-2 immune responses through releasing some cytokines and chemokines such as TGF-β, IL-4 and IL-13 which are involved in tissue repair and ECM deposition [26].

The induction of pulmonary fibrosis by $PM_{2.5}$ in the present study was histologically confirmed by increases in airway collagen deposition and fibrosis scores but with no change in alveolar mean linear intercept (Lm) in lung tissue which indicates the absence of emphysema. Persistent $PM_{2.5}$ exposure has been associated with reduced lung function indices, such as FVC, FEV1, and peak expiratory flow (PEF), in the young and the elderly[27, 28]. The present study showed that there were maximal decreases in IC, TLC and lung compliance (Cchord) in 9-week $PM_{2.5}$-instilled mice, which is probably due to lung fibrosis with features of restrictive lung volume and declined lung resilience indicating reduced lung capacity. As we also observed the fibrosis extending to the airways, our model is in addition a representative of airflow limitation caused by $PM_{2.5}$.

Collagen fibers, the primary components of fibrotic matrix, play an important role in airway remodeling and fibrous scar formation. Type I collagen is the major component in ECM, and is composed of two α1 and one α2 polypeptide chains [29]. Type III collagen is a minor component and forms thin fibrils. Therefore, type I collagen contents can indicate the severity of pulmonary fibrosis. As shown in the Sirius red-stained lung sections, there was an increase in the type I collagen deposition in airway walls and alveolar septum in 9-week $PM_{2.5}$-instilled mice. Type I pro-collagen polypeptides contain a continuous Gly-X-Y (X is frequently proline and Y is frequently hydroxyproline) repeat motif, which maintains type I collagen formation by hydroxylation and glycosylation [30]. As from 6 weeks of $PM_{2.5}$ instillation onwards, increased hydroxyproline concentrations were observed in mouse lung tissues, in line with the increased percentage area of type I collagen deposition.

In mammalian cells, mitochondrial fission is mediated mainly by DRP1 and MFF, while mitochondrial fusion is controlled by OPA1 and MFN1/2 [13]. Acute $PM_{2.5}$ exposure has been reported to induce the impairment of mitochondrial dynamics, as indicated by increased mitochondrial fission proteins and decreased mitochondrial fusion proteins [16]. In the early stage of $PM_{2.5}$ instillation, DRP1 and MFF were increased and OPA1 and MFN2 remained stable. With repeated $PM_{2.5}$ instillation, OPA1 and MFN2 were decreased, which indicated a decrease in mitochondrial fusion. Dysfunctional mitochondrial dynamics can have a significant impact on the mitophagic process. In response to damaged mitochondria, PINK1, a mitophagy regulator protein, accumulates on the outer mitochondrial membrane, recruiting Parkin, a cytosolic E3 ubiquitin ligase, to mitochondria [31]. Subsequently, Parkin ubiquitinates and degrades MFN1/2, and connects to LC3B II through adaptor protein SQSTM1/p62, which leads to autophagosome formation and mitophagy [31]. The process of mitophagy removes damaged mitochondria to maintain a

healthy mitochondrial pool, but an excessive rate of mitophagy may induce the reduction of mitochondrial quantity, the inhibition of mitochondrial respiratory function and bioenergy production, and the increase of mtROS levels [32]. In our study, 9-week of $PM_{2.5}$ instillation enhanced mitophagy and autophagy, as indicated by increased expression of Parkin and SQSTM1/p62, and enhanced ratio of LC3B II to LC3B I.

As a molecular reprogramming process, the activation of EMT by TGFβ in lung tissues is indicated by the loss of cell-cell adhesion molecule CDH1 (E-Cadherin), and the gain of mesenchymal markers including CDH2 (N-Cadherin), Vimentin and α-smooth muscle actin (α-SMA) in epithelial cells [33]. The EMT activation in the present study was evidenced by increased N-Cadherin and Vimentin expression and reduced E-Cadherin expression. Moreover, enhanced expression of TGFβ1 could activate PI3K-Akt pathways [9, 34], whilst inhibition of PI3K improved BLM-induced pulmonary fibrosis [35]. Knockout of Akt protected mice from chronic hypoxia-induced pulmonary vascular and tissue remodeling, and Akt inhibition also ameliorated adenovirus TGFβ (adTGFβ)-induced pulmonary fibrosis [36]. The increased Akt activation and ROS production could facilitate mitophagy which may prevent macrophage apoptosis, promote macrophage-derived TGFβ and stimulate inherent fibroblast activation and proliferation [37]. The increased expression of TGFβ1 protein with increased EMT and up-regulated phosphorylation levels of PI3K and Akt were demonstrated in the 9-week of $PM_{2.5}$ instilled mouse model.

NOX4 is the only member of NADPH oxidase family which is localized in mitochondria, and contributes to mtROS levels [38]. NOX4 can be stimulated by TGFβ1-SMAD2/3 pathways to catalyze the production of ROS, and can drive fibroblast proliferation and differentiation [39, 40]. Levels of NOX4 are elevated in lung tissue from patients with IPF and BLM-induced mouse models of pulmonary fibrosis [39, 40]. Inhibition of NOX4 activity attenuated the fibrotic response, as reflected in the reduction of collagen, fibronectin and TGFβ1, and the inhibition of EMT [41]. In the present study, there was increased expression of NOX4, accompanied by the elevation of mtROS levels in lung tissues starting from 3 weeks of $PM_{2.5}$ instillation. mtROS can then cause NLRP3 inflammasome activation which is capable of initiating lung inflammation[42, 43]. In addition, NLRP3 inflammasome activation accelerated the process of EMT, and eventually induced pulmonary fibrosis [44, 45].

In summary, intranasal instillation of $PM_{2.5}$ for 9 weeks induced lung inflammation and pulmonary fibrosis phenotype in mice, and possibly through driving EMT, mitochondrial damage and mitophagy, as well as activating TGFβ1-PI3K/Akt, TGFβ1-NOX4-NLRP3 pathways. Which pathways are important for the induction of fibrosis will be the subject of future studies using this $PM_{2.5}$-induced lung fibrosis model.

Abbreviations

$PM_{2.5}$: Fine particulate matter; IPF: Idiopathic pulmonary fibrosis; ROS: Reactive oxygen species; EMT: Epithelial–mesenchymal transition; TGFβ: Transforming growth factor β ; NOX4: NADPH oxidase 4; TOC:

Total organic carbon; PAHs: Poly aromatic hydrocarbons; BAL: Bronchoalveolar lavage; IC: Inspiratory capacity; TLC: Total lung capacity; FVC: Forced vital capacity; Cchord: chord compliance; MDA: Malondialdehyde; OPA1: Optic atrophy 1; MFN2: Mitofusion-2; DRP1: Dynamin-related protein 1; MFF: Mitochondrial fission factor

Declarations

Acknowledgements

We would like to thank Mr.Wenjun Huang of Shanghai Jiao Tong University, School of Environmental Science and Engineering for analyzing constitutes of $PM_{2.5}$.

Authors' contributions

Mengmeng Xu and Feng Li designed the experiments, co-wrote the paper and contributed to data analysis and interpretation. Mengmeng Xu, Hai Zhang and Lu Xu performed most experimental work. Hai Zhang, Xiaohui Wang and Chenfei Li participate in $PM_{2.5}$ extraction and Lung function detection. Yuqing Chen, Kian Fan Chung and Ian M Adcock help us review and edit the manuscript. Feng Li was in charge of the project administration and funding acquisition. All authors read and approved the final manuscript.

Funding

This work was supported by the Key International (Regional) Cooperative Project of National Natural Science Foundation of China (No.51420105010), The Action Plan for Science and Technology Innovation of Shanghai Municipal Commission of Science and Technology (15140903400), SMC-Chenxing Award Project from Shanghai Jiao Tong University (DY22.05041601)

Availability of data and materials

The data and materials used to support the findings of this study are available from the corresponding author upon request.

Ethics approval and consent to participate

All experimental studies involved mice were approved by the laboratory animal ethics committee of the Shanghai Chest Hospital, Shanghai, China (Approval number: SYXK 2018-0016).

Competing interests

All authors declare no competing interests to disclosure.

References

1. Raghu G, Remy-Jardin M, Myers JL, et al. Diagnosis of Idiopathic Pulmonary Fibrosis. An Official ATS/ERS/JRS/ALAT Clinical Practice Guideline. Am J Respir Crit Care Med. 2018;198:e44-e68.
2. Hutchinson J, Fogarty A, Hubbard R, McKeever T. Global incidence and mortality of idiopathic pulmonary fibrosis: a systematic review. Eur Respir J. 2015;46:795-806.
3. Raghu G, Chen SY, Yeh WS, et al.Idiopathic pulmonary fibrosis in US Medicare beneficiaries aged 65 years and older: incidence, prevalence, and survival, 2001-11. Lancet Respir Med. 2014;2:566-72.
4. Siroux V, Crestani B. Is chronic exposure to air pollutants a risk factor for the development of idiopathic pulmonary fibrosis? Eur Respir J, 2018;51: 1702663.
5. Sesé L, Nunes H, Cottin V, et al. Role of atmospheric pollution on the natural history of idiopathic pulmonary fibrosis. Thorax. 2018;73:145-150.
6. Camelo A, Dunmore R, Sleeman MA, et al. The epithelium in idiopathic pulmonary fibrosis: breaking the barrier. Front Pharmacol. 2014;4:173.
7. Bagnato G, Harari S. Cellular interactions in the pathogenesis of interstitial lung diseases. Eur Respir Rev. 2015;24:102-14.
8. Saito A, Horie M, Nagase T. TGF-β Signaling in Lung Health and Disease. Int J Mol Sci. 2018;19:2460.
9. Woodcock HV, Eley JD, Guillotin D, et al. The mTORC1/4E-BP1 axis represents a critical signaling node during fibrogenesis. Nat Commun. 2019;10:6.
10. Stock CJW, Michaeloudes C, Leoni P, et al. Bromodomain and Extraterminal (BET) Protein Inhibition Restores Redox Balance and Inhibits Myofibroblast Activation. Biomed Res Int. 2019;2019:1484736.
11. Li Y, Li H, Liu S, et al. Pirfenidone ameliorates lipopolysaccharide-induced pulmonary inflammation and fibrosis by blocking NLRP3 inflammasome activation. Mol Immunol. 2018;99:134-144.
12. Zank DC, Bueno M, Mora AL, et al. Idiopathic Pulmonary Fibrosis: Aging, Mitochondrial Dysfunction, and Cellular Bioenergetics. Front Med (Lausanne). 2018;5:10.
13. Hara H, Kuwano K, Araya J. Mitochondrial Quality Control in COPD and IPF. Cells. 2018;7:86.
14. Bueno M, Lai YC, Romero Y, et al. PINK1 deficiency impairs mitochondrial homeostasis and promotes lung fibrosis. J Clin Invest.2015;125:521-38.
15. Falcon-Rodriguez CI, Osornio-Vargas AR, Sada-Ovalle I, et al. Aeroparticles, Composition, and Lung Diseases. Front Immunol. 2016;7:3.
16. Xu M, Zhang Y, Wang M,et al. TRPV1 and TRPA1 in Lung Inflammation and Airway Hyperresponsiveness Induced by Fine Particulate Matter ($PM_{2.5}$). Oxid Med Cell Longev. 2019, 2019:7450151.
17. Liu S, Zhang W, Zhang F, et al. TMT-Based Quantitative Proteomics Analysis Reveals Airborne PM2.5-Induced Pulmonary Fibrosis. Int J Environ Res Public Health. 2018;16:98.
18. Xu Z, Li Z, Liao Z, et al. PM2.5 induced pulmonary fibrosis in vivo and in vitro. Ecotoxicol Environ Saf. 2019;171:112-121.

19. Li F, Wiegman CH, Seiffert J, et al. Effects of N-acetylcysteine in ozone-induced model of chronic obstructive pulmonary disease. PLoS One. 2013;8:e80782.
20. Szapiel SV, Elson NA, Fulmer JD, et al.Bleomycin-induced interstitial pulmonary disease in the nude, athymic mouse. Am Rev Respir Dis. 1979;120:893-9.
21. Hübner RH, Gitter W, El Mokhtari NE, et al. Standardized quantification of pulmonary fibrosis in histological samples. Biotechniques. 2008;44:507-517.
22. Chen C, Yun XJ, Liu LZ, et al. Exogenous nitric oxide enhances the prophylactic effect of aminoguanidine, a preferred iNOS inhibitor, on bleomycin-induced fibrosis in the lung: Implications for the direct roles of the NO molecule in vivo. Nitric Oxide. 2017;70:31-41.
23. Jenkins RG, Moore BB, Chambers RC, et al. An Official American Thoracic Society Workshop Report: Use of Animal Models for the Preclinical Assessment of Potential Therapies for Pulmonary Fibrosis. Am J Respir Cell Mol Biol. 2017;56:667-679.
24. Tashiro J, Rubio GA, Limper AH, et al. Exploring Animal Models That Resemble Idiopathic Pulmonary Fibrosis. Front Med (Lausanne). 2017;4:118.
25. Braga TT, Agudelo JS, Camara NO. Macrophages During the Fibrotic Process: M2 as Friend and Foe. Front Immunol. 2015;6:602.
26. Puttur F, Gregory LG, Lloyd CM. Airway macrophages as the guardians of tissue repair in the lung. Immunol Cell Biol. 2019;97:246-257.
27. Bergstra AD, Brunekreef B, Burdorf A. The effect of industry-related air pollution on lung function and respiratory symptoms in school children. Environ Health. 2018;17:30.
28. Chu H, Xin J, Yuan Q, et al. Evaluation of vulnerable PM2.5-exposure individuals: a repeated-measure study in an elderly population. Environ Sci Pollut Res Int. 2018;25:11833-11840.
29. Urban ML, Manenti L, Vaglio A. Fibrosis–A Common Pathway to Organ Injury and Failure. N Engl J Med. 2015;373:95-6.
30. Zhang Y, Stefanovic B. LARP6 Meets Collagen mRNA: Specific Regulation of Type I Collagen Expression. Int J Mol Sci. 2016;17:419.
31. Pickles S, Vigié P, Youle RJ. Mitophagy and Quality Control Mechanisms in Mitochondrial Maintenance.Curr Biol. 2018;28:R170-R185.
32. Zhang ZQ, Zhang CZ, Shao B, et al. Effects of abnormal expression of fusion and fission genes on the morphology and function of lung macrophage mitochondria in SiO_2-induced silicosis fibrosis in rats in vivo. Toxicol Lett. 2019;312:181-187.
33. Jolly MK, Ward C, Eapen MS, et al. Epithelial-mesenchymal transition, a spectrum of states: Role in lung development, homeostasis, and disease. Dev Dyn. 2018;247:346-358.
34. Saito S, Zhuang Y, Shan B,et al. Tubastatin ameliorates pulmonary fibrosis by targeting the TGFbeta-PI3K-Akt pathway. PLoS One. 2017;12:e0186615.
35. Hsu HS, Liu CC, Lin JH, et al. Involvement of ER stress, PI3K/AKT activation, and lung fibroblast proliferation in bleomycin-induced pulmonary fibrosis. Sci Rep. 2017;7:14272.

36. Abdalla M, Sabbineni H, Prakash R,et al. The Akt inhibitor, triciribine, ameliorates chronic hypoxia-induced vascular pruning and TGF beta-induced pulmonary fibrosis. Br J Pharmacol. 2015;172:4173-88.
37. Larson-Casey JL, Deshane JS, Ryan AJ, et al. Macrophage Akt1 Kinase-Mediated Mitophagy Modulates Apoptosis Resistance and Pulmonary Fibrosis. Immunity. 2016;44:582-596.
38. Giardino G, Cicalese MP, Delmonte O, et al. NADPH Oxidase Deficiency: A Multisystem Approach. Oxid Med Cell Longev. 2017;2017:4590127.
39. Guo W, Saito S, Sanchez CG, et al. TGF-β1 stimulates HDAC4 nucleus-to-cytoplasm translocation and NADPH oxidase 4-derived reactive oxygen species in normal human lung fibroblasts. Am J Physiol Lung Cell Mol Physiol. 2017;312:L936-L944.
40. Ghatak S, Hascall VC, Markwald RR, et al. Transforming growth factor β1 (TGFβ1)-induced CD44V6-NOX4 signaling in pathogenesis of idiopathic pulmonary fibrosis. J Biol Chem. 2017;292:10490-10519.
41. Jarman ER, Khambata VS, Cope C,et al. An inhibitor of NADPH oxidase-4 attenuates established pulmonary fibrosis in a rodent disease model.Am J Respir Cell Mol Biol. 2014;50:158-69.
42. Zhou R, Yazdi AS, Menu P, et al. A role for mitochondria in NLRP3 inflammasome activation. Nature. 2011;469:221–225.
43. Li F, Xu M, Wang M,et al.Roles of mitochondrial ROS and NLRP3 inflammasome in multiple ozone-induced lung inflammation and emphysema. Respir Res. 2018;19:230.
44. Lv Z, Wang Y, Liu YJ,et al.NLRP3 Inflammasome Activation Contributes to Mechanical Stretch-Induced Endothelial-Mesenchymal Transition and Pulmonary Fibrosis. Crit Care Med. 2018;46:e49-e58.
45. Tian R, Zhu Y, Yao J,et al. NLRP3 participates in the regulation of EMT in bleomycin-induced pulmonary fibrosis. Exp Cell Res. 2017;357:328-334.

Figures

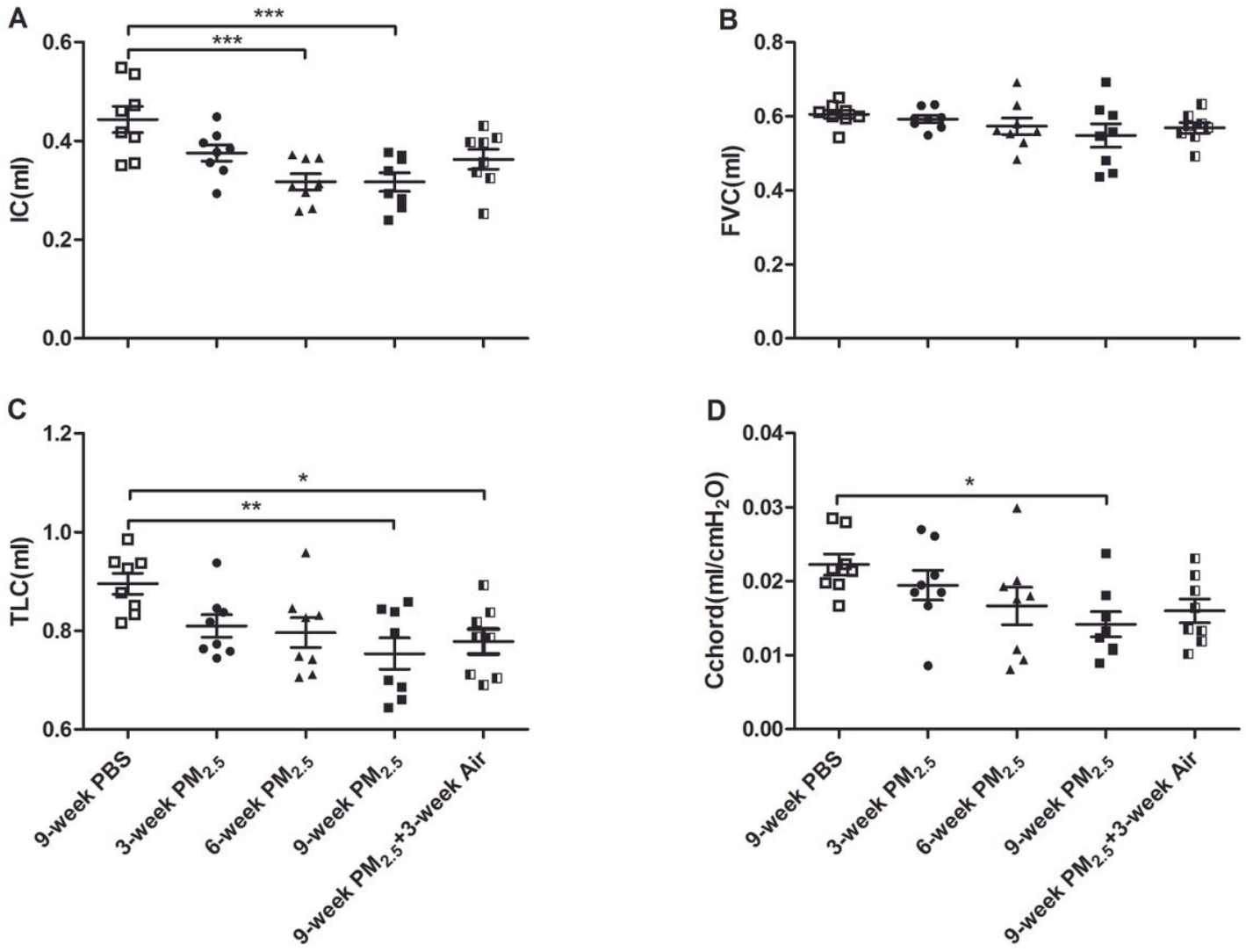

Figure 1

Effect of PM2.5 on lung function in mice. Individual and mean values of inspiratory capacity (IC) (A), forced volume capacity (FVC) (B), total lung capacity (TLC) (C), and chord compliance (Cchord) (D). *P<0.05, **P<0.01, ***P<0.001 compared with 9-week PBS-instilled mice.

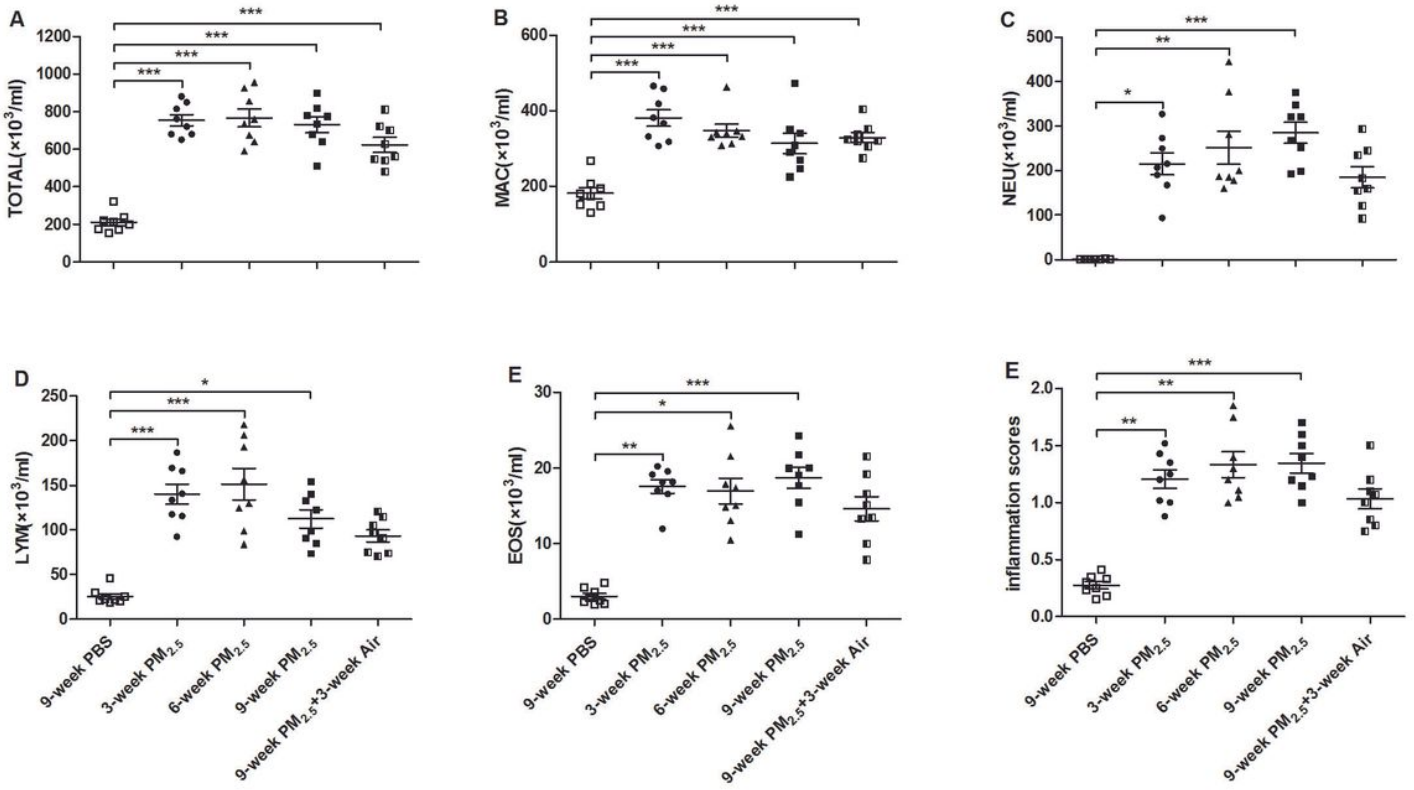

Figure 2

Effect of PM2.5 on BAL fluid inflammatory cells in mice. Individual and mean numbers of total cells (TOTAL) (A), macrophages (MAC) (B), neutrophils (NEU) (C), lymphocytes (LYM) (D), and eosinophils (EOS) (E) in BAL fluid. Individual and mean values of inflammation scores in airway walls and alveolar septa in mouse lung tissues (F). *P<0.05, **P<0.01, ***P<0.001 compared with 9-week PBS-instilled mice.

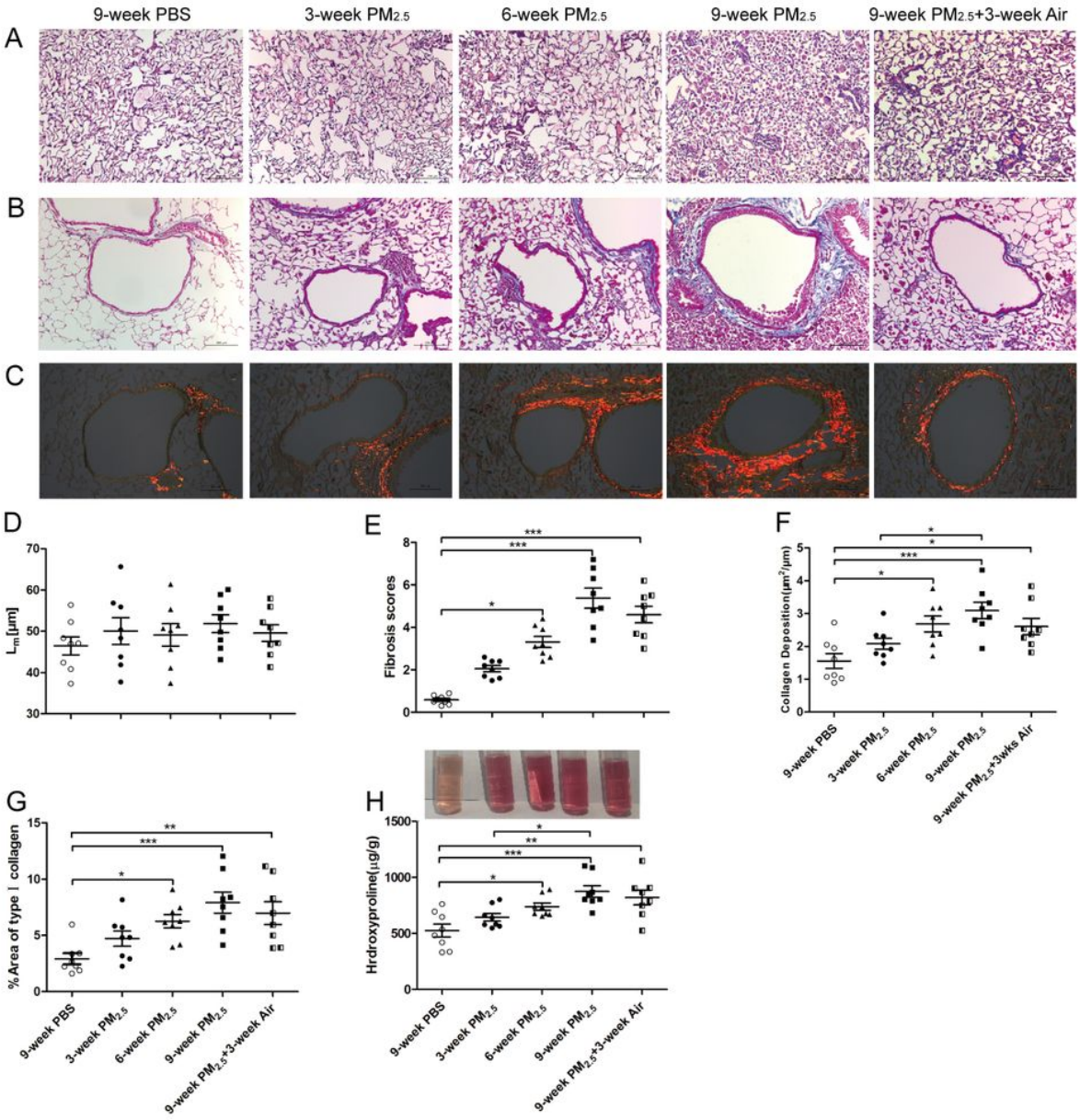

Figure 3

Effect of PM2.5 on lung histopathology and hydroxyproline contents in mice. Representative alveolar spaces of mouse lung tissues in hematoxylin and eosin-stained sections (A), bars 100μm. Representative bronchial photomicrographs in Masson trichrome-stained sections (B), bars 100μm. Representative bronchial photomicrographs in Sirius red-stained sections (C), bars 100μm. Individual and mean values of mean linear intercept (Lm) (D) and pulmonary fibrosis scores (E) measured from H&E-stained sections. Individual and mean values of collagen deposition thickness (μm2/μm) in the airway subepithelium (F) measured from Masson trichrome-stained sections. Individual and mean %area of the type I collagen deposition in lung tissues measured from Sirius red-stained sections (G). Alkalinehydrolysis assay of individual and mean contents of hydroxyproline in mouse lung tissues (H). *P<0.05, **P<0.01, ***P<0.001 compared with 9-week PBS-instilled mice.

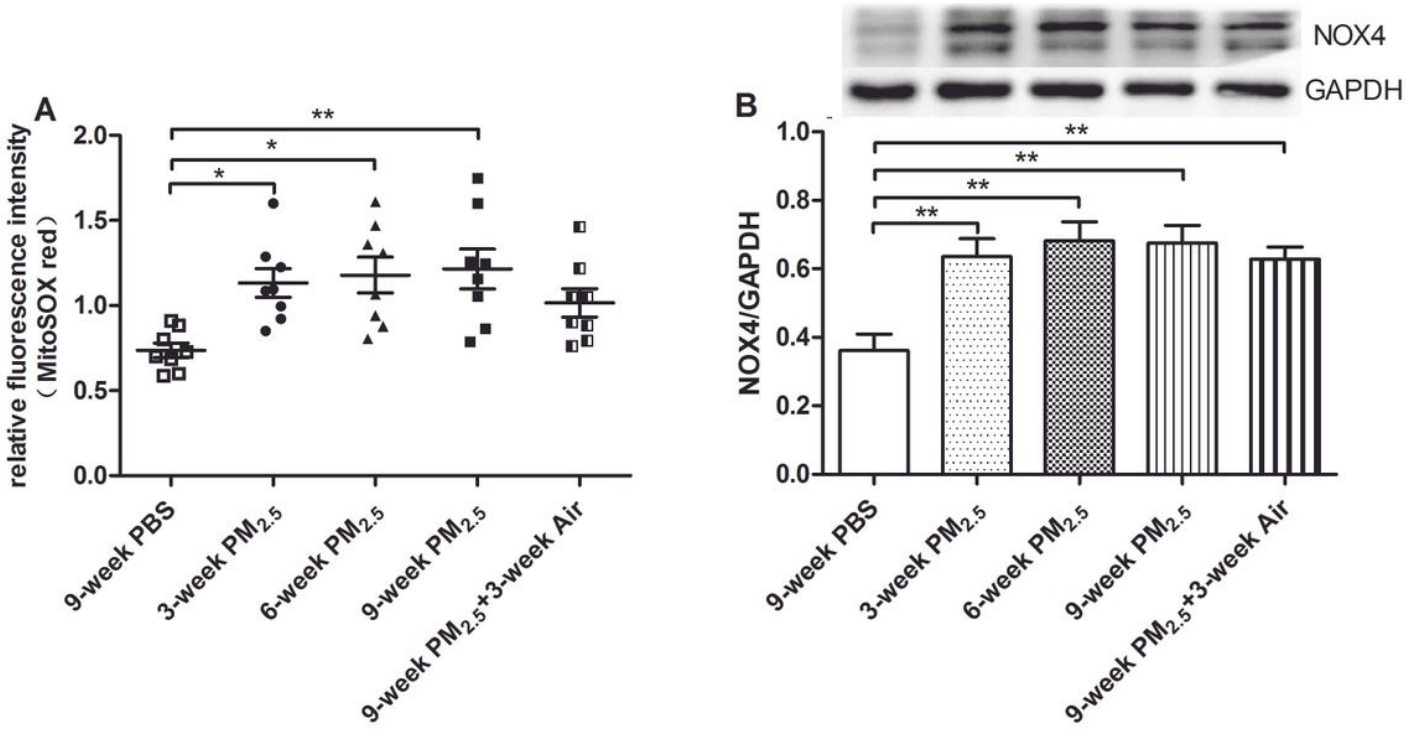

Figure 4

Effect of PM2.5 on levels of oxidative stress in mice. The individual and mean relative fluorescence intensity of mtROS in the mitochondrial suspension extracted from mouse lung tissues (A). Western blot analysis of the relative protein expression of NADPH oxidase 4 (NOX4) to GAPDH in the lung tissues (B). Each panel shows a representative Western blot. *P<0.05, **P<0.01, ***P<0.001 compared with 9-week PBS-instilled mice.

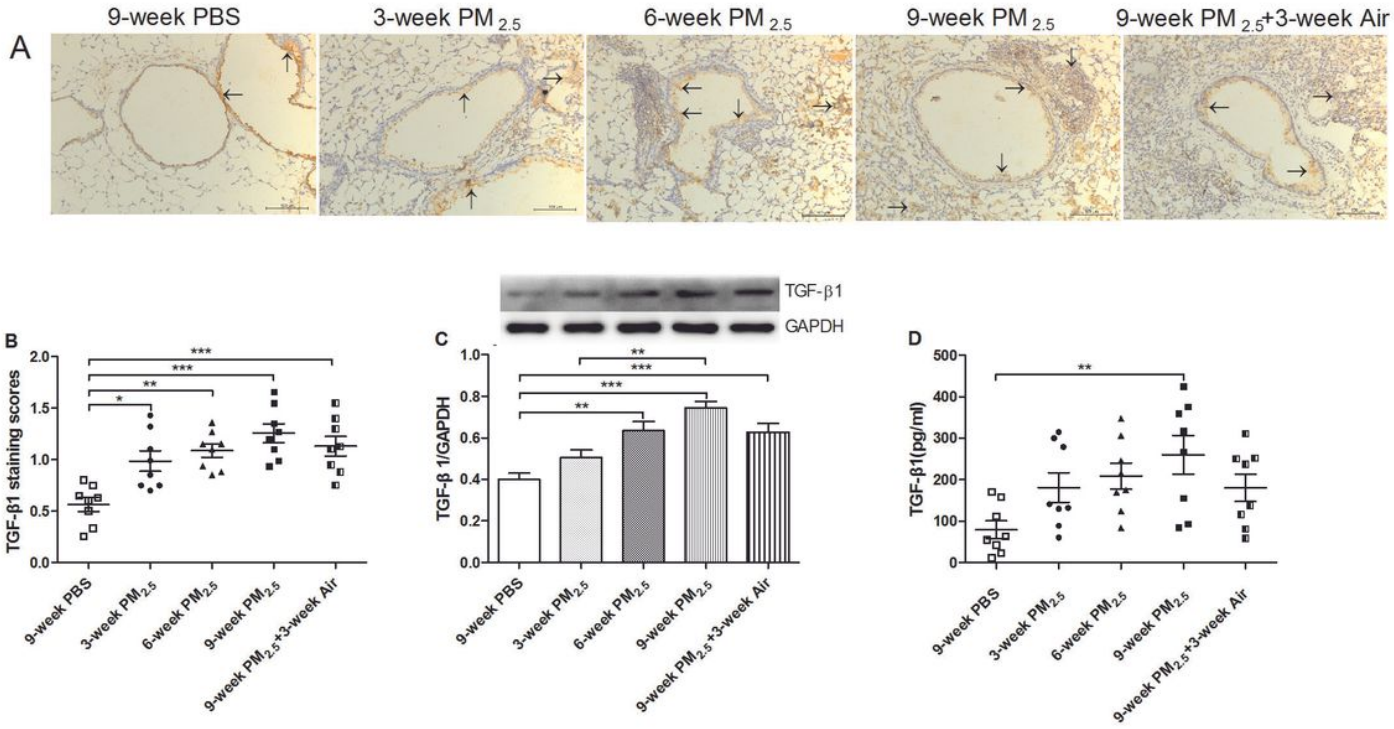

Figure 5

Effect of PM2.5 on expressed levels of TGFβ1 in mice. Representative immunohistochemical (IHC) staining for TGFβ1 as indicated by the brown staining (black arrows) in mouse lung tissue sections (A), bars 100μm. Individual and mean immunostaining scores of TGFβ1 measured by lung immunohistochemical sections (B). Western blot analysis of the relative protein expression of TGFβ1 to GAPDH in mouse lung tissue homogenates (C). Each panel shows a representative Western blot. Individual and mean levels of TGFβ1 in mouse serum (D). *P<0.05, **P<0.01, ***P<0.001 compared with 9-week PBS-instilled mice.

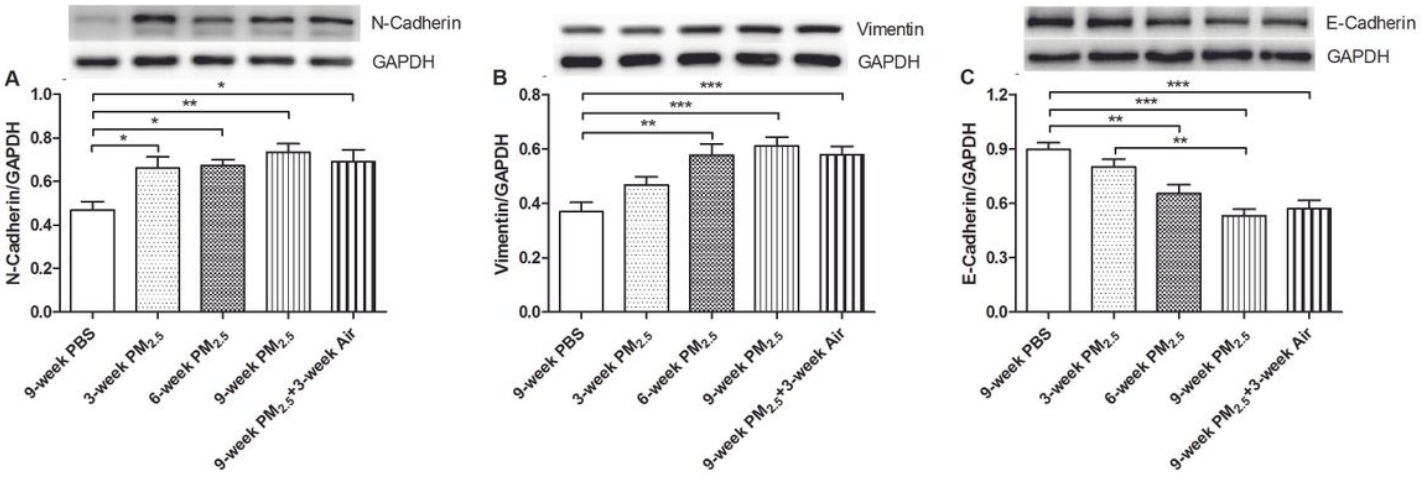

Figure 6

Effect of PM2.5 on Epithelial-mesenchymal transition (EMT) in mice. Western blot analysis of the relative protein expression ratio of N-Cadherin (A), Vimentin (B) and E-Cadherin (C) to GAPDH in mouse lung tissues. Each panel shows a representative Western blot. *P<0.05, **P<0.01, ***P<0.001 compared with 9-week PBS-instilled mice.

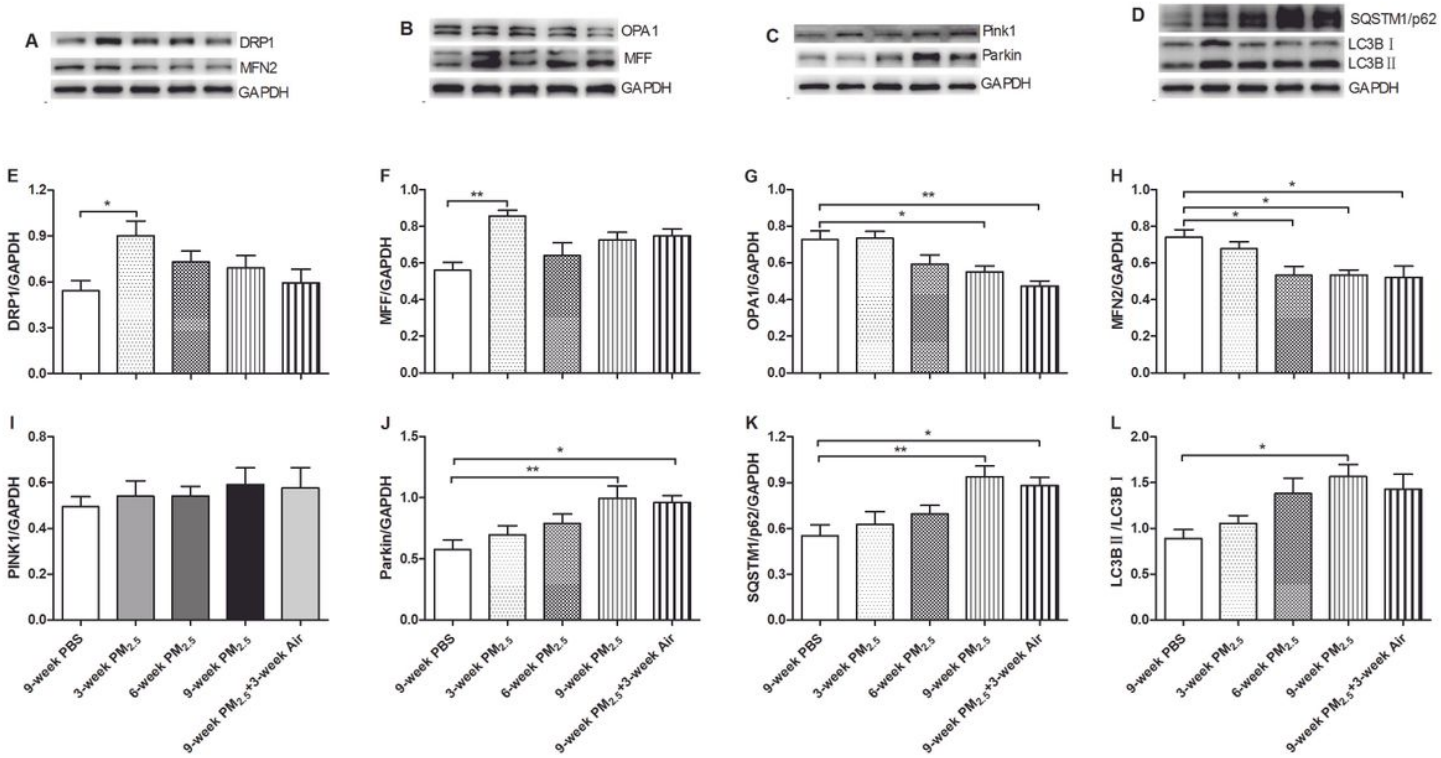

Figure 7

Effect of PM2.5 on Mitochondrial fission/fusion and mitophagy in mice. Western blot analysis of the relative protein expression ratio of Dynamin-related protein 1 (DRP1) (A, E), Mitofusin 2 (MFN2) (A, F), Optic Atrophy 1 (OPA1) (B, G), Mitochondrial fission factor (MFF) (B, H), PINK1 (C, I), Parkin (C, J) and SQSTM1/p62 (D, K) to GAPDH, the ratio of LC3BII to LC3BI (D, L) in mouse lung tissues. *P<0.05, **P<0.01, ***P<0.001 compared with 9-week PBS-instilled mice.

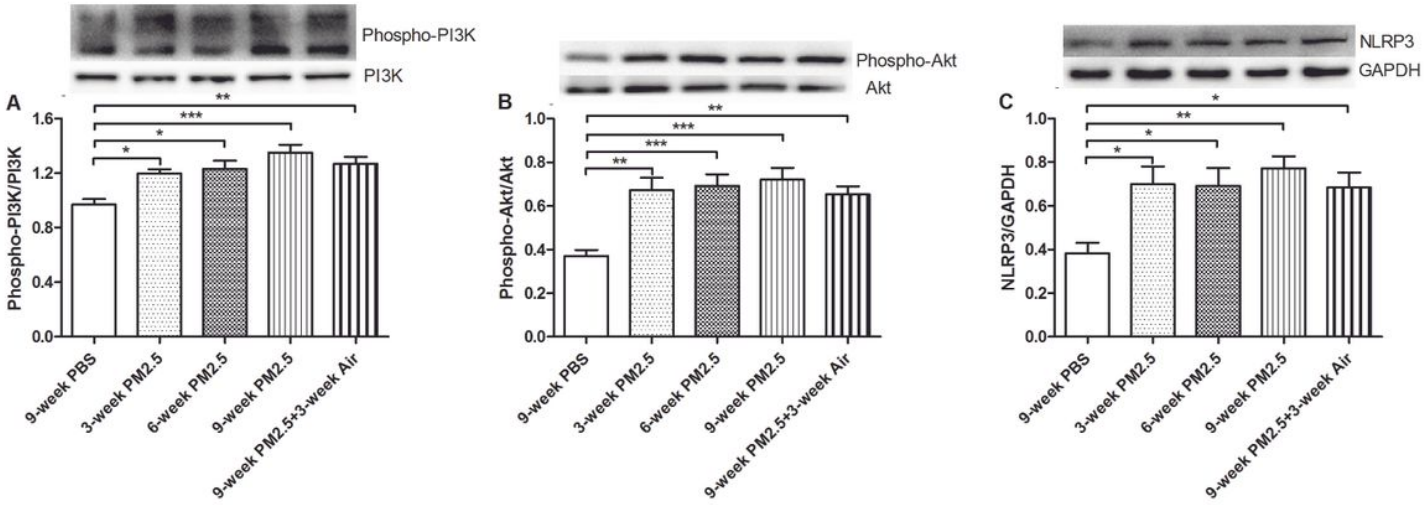

Figure 8

Effect of PM2.5 on PI3K/Akt phosphorylation and NLRP3 expression in mice. Western blot analysis of the ratio of phosphrylated-PI3k to total PI3K (A) and phosphorylated-Akt to total Akt (B), and relative protein expression ratio of NLRP3 to GAPDH (C) in mouse lung tissues. Each panel shows a representative Western blot. *P<0.05, **P<0.01, ***P<0.001 compared with 9-week PBS-instilled mice.

Supplementary Files

This is a list of supplementary files associated with this preprint. Click to download.

- Graphicalabstract.tif